Journal of Catalysis **210,** 418–430 (2002)
doi:10.1006/jcat.2002.3686

Spectroscopic Study on the Irreversible Deactivation of Chromia/Alumina Dehydrogenation Catalysts

Riikka L. Puurunen[1,2] and Bert M. Weckhuysen[3]

Centrum voor Oppervlaktechemie en Katalyse, Departement Interfasechemie, K.U.Leuven, Kasteelpark Arenberg 23, B-3001 Leuven, Belgium

Received March 4, 2002; revised May 17, 2002; accepted May 23, 2002

Irreversible deactivation of chromia/alumina dehydrogenation catalysts was investigated by deactivating the catalysts (4 wt% Cr) through prolonged calcination in air at temperatures up to 1200°C. Nitrogen physisorption, X-ray diffraction, diffuse reflectance spectroscopy in the UV–visible region, X-ray photoelectron spectroscopy, electron spin resonance spectroscopy, and catalytic measurements revealed that two deactivation mechanisms were responsible for the formation of catalytically inactive alumina-incorporated Cr^{3+} species: (i) entrapment of Cr^{3+} ions inside the alumina support during sintering of the alumina support and (ii) migration of Cr^{3+} ions into the alumina support. Chromia that had been impregnated on alumina inhibited the phase transformation from γ- to α-alumina. The presence of γ-alumina, in turn, hindered the migration of Cr^{3+} ions into alumina. The turnover frequency was higher for multinuclear Cr^{3+} than for isolated Cr^{3+} sites. The phase of the alumina support did not appear to affect the activity of the surface Cr^{3+} species.

Key Words: **chromia/alumina catalysts; alkane dehydrogenation; irreversible deactivation.**

INTRODUCTION

The catalytic dehydrogenation of alkanes is of great importance as an effective route for the production of propene and other light alkenes (1–4). Chromia/alumina catalysts are industrially used for this process, and much recent research has been devoted to elucidating the structures of alumina-supported chromium oxide (5–24). Despite these efforts, there is no consensus on the origin of the catalytic activity or on the deactivation mechanisms. In the following we first summarize qualitatively the structures of chromium known to be present in chromia/alumina catalysts and then we define some unanswered questions regarding this complex catalyst system.

[1] To whom correspondence should be addressed. Fax: +358 9 451 2622. E-mail: riikka.puurunen@hut.fi.

[2] Current address: Helsinki University of Technology, Laboratory of Industrial Chemistry, P.O. Box 6100, FIN-02015 HUT, Finland.

[3] Current address: Utrecht University, Debye Institute, Department of Inorganic Chemistry and Catalysis, P.O. Box 80083, NL-3508 TC Utrecht, The Netherlands.

Oxidized chromia/alumina catalysts contain chromium in oxidation states Cr^{6+}, Cr^{5+}, and Cr^{3+} (5–23). Cr^{6+} and Cr^{5+} are reduced by alkanes, hydrogen, and carbon monoxide under typical dehydrogenation conditions (500–600°C) (5–8, 10–13, 16, 19, 21, 23). Oxidation state Cr^{3+} has most often been proposed as the state existing after reduction (5–8, 10–13, 16, 19, 21, 23); some Cr^{5+} may remain after reduction with hydrogen (25) and part of the chromium may reduce to Cr^{2+} (13). Figure 1a shows one way of classifying the different types of Cr^{3+} species that are present in reduced chromia/alumina catalysts. Type 1 sites are surface Cr^{3+} sites, with subclasses type 1′ and type 1″, which are presumably catalytically active. A type 1′ site is an isolated (i.e., mononuclear) Cr^{3+} ion that does not interact with other chromium sites; it is sometimes referred to as dispersed Cr^{3+} (18). A type 1″ site is a Cr^{3+} ion that has one or more neighboring Cr^{3+} ions and thus is called multinuclear Cr^{3+}. Type 1″ sites are also called "Cr^{3+} clusters." In addition there are type 2 and type 3 sites, where the Cr^{3+} is not a surface ion but is buried inside chromia crystallites (type 2) or the alumina support (type 3). Since types 2 and 3 are not surface species, they are not catalytically active. Chromia crystallites consist of type 1″ and type 2 sites together and may grow in size so that they become visible in X-ray diffraction (XRD).

The Cr^{3+} species have also been classified in terms of origin (7, 10–12). Those Cr^{3+} ions that have been formed through reduction of chromium in high oxidation states (Cr^{6+} and Cr^{5+}) in a reducing atmosphere are referred to as "redox Cr^{3+}," whereas those Cr^{3+} ions that have been stabilized as Cr^{3+} are referred to as "nonredox Cr^{3+}." Redox Cr^{3+} is exposed on the surface and thus can be catalytically active. Nonredox Cr^{3+} may be exposed and catalytically active, but it may also be buried inside chromia crystallites or inside the alumina support and thus be catalytically inactive. Redox Cr^{3+} is abundant in chromia/alumina catalysts with low chromium loading, whereas nonredox is Cr^{3+} mostly present in catalysts with higher loadings (10).

Figure 1b shows how the classifications in terms of type and origin overlap. Since Cr^{6+} and Cr^{5+} sites are often isolated on the alumina surface, type 1′ sites and redox Cr^{3+}

0021-9517/02 $35.00

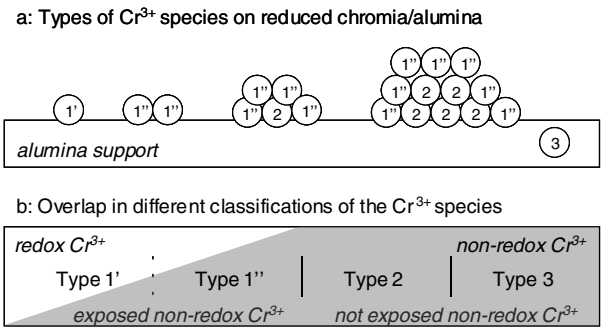

FIG. 1. (a) Schematic summary of the different Cr^{3+} species present on reduced chromia/alumina catalysts (oxygen ions between the Cr^{3+} ions are omitted for clarity), and (b) an illustration of the overlap in the different classifications of Cr^{3+} species.

are largely the same. However, UV–visible near-infrared diffuse reflectance spectroscopy (UV–vis NIR DRS), electron spin resonance spectroscopy (ESR), and Raman spectroscopy have shown that Cr^{6+} and Cr^{5+} ions present on oxidized chromia/alumina catalysts may have neighboring chromium ions (26, 27). Thus, some redox Cr^{3+} probably falls in the category of type 1″ sites. Exposed nonredox Cr^{3+} should be mostly classified as type 1″ with minor contributions from type 1′ sites, and nonexposed nonredox Cr^{3+} should be classified as type 2 or type 3 sites.

Several questions need to be addressed in regard to the chromia/alumina dehydrogenation catalysts. Do the catalytic activity and rate of deactivation of the various Cr^{3+} sites differ (7, 10, 12, 25)? Is Cr^{2+} present in chromia/alumina dehydrogenation catalysts (13)? Does the phase of the alumina support affect the catalytic activity of chromia (19)? Industrial chromia/alumina catalysts have a high chromium loading of about 15 at_{Cr}/nm^2 (1). Can relevant information on the active sites be gained by studying catalysts with low chromium loadings (6, 12, 13)? When used under cycling of severe oxidizing and reducing conditions over a period of years in industrial operations, chromia/alumina catalysts deactivate through the formation of solid solutions of chromia–alumina (1, 3). How does the irreversible deactivation occur?

The main interest in the present work is the physicochemical processes leading to irreversible deactivation of chromia/alumina catalysts. For this purpose, chromia was supported on alumina containing various amounts of γ-, θ-, or α-alumina. The catalysts were calcined at different temperatures (600, 900, 1000, 1100, and 1200°C) in order to generate catalytically inactive Cr^{3+} species (21). On the basis of studies by nitrogen physisorption, XRD, UV–vis DRS, X-ray photoelectron spectroscopy (XPS), and ESR, we propose a model describing the deactivation process in terms of catalyst-support sintering and chromium migration. In addition, we discuss the effect of the alumina support on the deactivation and the catalytic activity of the various Cr^{3+} species.

EXPERIMENTAL

Catalyst Preparation

Chromia/alumina samples with 4 wt% Cr were chosen to evaluate the effect of alumina precalcination temperature and catalyst calcination temperature on dehydrogenation activity. At this loading, high dehydrogenation selectivities should be obtained (10), and at the same time spectroscopic characterization of the samples should be feasible. The samples were prepared by incipient wetness impregnation of CrO_3 (UCB chemicals, p.a.) from an aqueous solution onto a commercial alumina support (AKZO 001-1.5E) that had been pulverized with a ball mill. Alumina was precalcined in ambient air at 800, 1000, and 1200°C for 24 h to produce supports with different surface areas and crystalline phases. After impregnation, the samples were aged for 4 h and dried for 4 h at 60 and 120°C, respectively. The whole catalyst batch was then calcined at 600°C for 24 h; after this, part of it was removed, calcination was continued at 900°C for 24 h, part was removed, and so on, until the final part of the catalyst batch had been calcined at 1200°C for 24 h.

The samples are described in Table 1. In the following they are referred to with one- or two-numbered sample codes: the first number of the sample code indicates the alumina precalcination temperature and the second number the catalyst calcination temperature. Thus, sample **8** is a reference sample of alumina calcined at 800°C, while chromia/alumina catalyst **8-6** was prepared on alumina precalcined at 800°C and, thereafter, calcined at 600°C. Notations such as "**8-*** series" refer to samples **8-6**, **8-9**, **8-10**, **8-11**, and **8-12**.

Nitrogen Physisorption

Nitrogen adsorption isotherms were measured for the samples with Coulter Omnisorp 100 equipment. Samples were pretreated in vacuum at 400°C overnight. The surface areas were determined from the adsorption curve in the p/p_0 range 0.05–0.2 by the Brunauer–Emmett–Teller (BET) method. Pore volumes were determined from the desorption curve by the Barrett–Joyner–Hallender (BJH) method.

X-Ray Diffraction

The presence of different alumina and chromia phases was investigated by XRD. Diffractograms were measured by a Siemens D5000 matic X-Ray-Diffractometer, and the phases were identified with the database of Siemens Diffrac AT program (© 1993).

TABLE 1

Properties of Chromia/Alumina Catalysts with 4 wt% Cr

Sample code	Alumina precalcination temperature (°C)	Catalyst calcination temperature (°C)	Surface area (m^2/g)	Pore volume (ml/g)	Alumina phases detected by XRD	Total surface loading of Cr (at_{Cr}/nm^2)	Estimated surface loading of non-alumina-incorporated Cr^{3+} [a] (at_{Cr}/nm^2)
8	800	—[b]	177	0.82	γ	—	—
10	1000	—	106	0.68	(γ), θ, (α)	—	—
12	1200	—	41	0.36	(θ), α	—	—
8-6	800	600	186	0.73	γ	2.5	2.5
8-9	800	900	158	0.75	γ, (θ)	2.9	—
8-10	800	1000	120	0.76	(γ), θ	3.9	3.0
8-11	800	1100	98	0.71	(γ), θ	4.7	—
8-12	800	1200	75	0.56	(γ), θ, (α)	6.2	3.0
10-6	1000	600	110	0.62	(γ), θ, α	4.2	3.9
10-9	1000	900	102	0.67	(γ), θ, α	4.5	3.8
10-10	1000	1000	91	0.67	(γ), θ, α	5.1	3.9
10-11	1000	1100	82	0.60	(γ), θ, α	5.6	3.0
10-12	1000	1200	64	0.51	(γ), θ, α	7.2	2.8
12-6	1200	600	50	0.36	θ, α	9.3	6.9
12-9	1200	900	47	0.34	θ, α	9.9	—
12-10	1200	1000	48	0.36	θ, α	9.7	5.2
12-11	1200	1100	36	0.26	θ, α	12.9	—
12-12	1200	1200	29	0.20	θ, α	16.0	4.1

[a] Calculated by subtracting the fraction of alumina-incorporated Cr^{3+}, estimated from *ex situ* DRS results, from the total chromium content.
[b] Not applicable or not determined.

Propane Dehydrogenation Activity

The dehydrogenation activity of the catalyst samples was measured in a tubular fixed-bed reactor equipped with an *in situ* DRS facility (21). A fresh 0.2-g batch of catalyst, ground and pelletized to a particle size of 0.25–0.5 mm, was used for each run. Propane (Alpha Gas, 99.95 vol%) diluted to 10% with helium (Air Liquide, 99.995 vol%) was used as the feed. The catalyst was regenerated with 5% oxygen (Air Liquide, 99.5 vol%) in helium. Helium flushes separated dehydrogenation and regeneration. A flow rate of 25 cm^3/min was used. Three dehydrogenation cycles were carried out. A cycle consisted of a 20-min dehydrogenation, 30-min flush with helium, 40-min regeneration, and 20-min flush with helium. The outlet gases were analyzed online by a gas chromatograph (HP 5830A) equipped with a flame ionization detector and a packed column (*n*-octane/porasil c). Components eluted in the order methane, combination of ethane and ethene, propane, and propene. Samples were taken at 4 and 17 min from the start of the propane feed.

Conversion (X), yield (Y), and selectivity (S) were calculated on a molar basis as follows: $X = 100\% \cdot (F_{\text{propane,in}} - F_{\text{propane,out}})/F_{\text{propane,in}}$ (F_i is the molar flow of component i), $Y_i = 100\% \cdot F_{i,\text{out}}/F_{\text{propene,in}}$, and $S_i = 100\% \cdot Y_i/X$. The molar response factor of propene relative to propane was determined to be 1.08; the response factors published by Dietz (28) were used for other components. The results are presented for the second dehydrogenation cycle if not otherwise stated.

Ex Situ Diffuse Reflectance Spectroscopy

The coordination environment of Cr^{3+} in the chromia/alumina samples was investigated by UV–vis NIR DRS measurements carried out at room temperature under nitrogen atmosphere. To distinguish it from the *in situ* DRS measurements (see below), the UV–vis NIR DRS technique will be referred to as *ex situ* DRS. Spectra were collected with a Cary 5 UV–vis NIR spectrophotometer in the wavenumber range 50,000–4,000 cm^{-1}, from samples placed in a quartz cell equipped with a suprasil window. Spectra were measured for hydrated samples (that is, samples that were kept in ambient air), for samples oxidized in air at 550°C overnight, and for samples reduced thereafter in hydrogen at 550°C for about 4 h. The reduction step was needed to observe the positions of the d–d transitions of Cr^{3+} without the interfering effect of Cr^{6+} charge transfer bands. A commercial white reference, Labsphere SBS-99-010, was used. Spectra are shown in the Kubelka–Munk format (K–M $= (1 - R)^2/2R$; R = reflectance).

In Situ Diffuse Reflectance Spectroscopy

The oxidation state and coordination environment of chromium were investigated *in situ* during the dehydrogenation runs at 580°C by a fiberoptic *in situ* DRS setup that has been described previously (21). In the *in situ* DRS setup, light is directed to and collected from the catalyst bed by a fiberoptic probe that withstands high temperatures and

whose tip is in close contact with the catalyst bed. Spectra were collected in the UV–vis region in the wavenumber range 35,000–11,530 cm^{-1}. One scan was typically measured in 70 ms. About 10 or 1000 scans were averaged for one spectrum, depending on the desired rate of collecting spectra and on the signal-to-noise ratio. AKZO 001-1.5E alumina calcined at 800°C and crushed and sieved to a particle size of 0.25–0.50 mm was used as the white reference material.

Higher measurement temperature affects the DR spectrum: the Cr^{3+} d–d bands shift to lower energy and become wider and more intense (the band areas increase) (29, p. 360). Previous measurements (21, 30) with the same *in situ* setup showed that increase from room temperature to 580°C shifts the d–d transitions of Cr^{3+} at about 17,000 and 22,000 cm^{-1} to lower energy by about 700 and 200 cm^{-1}.

X-Ray Photoelectron Spectroscopy

The relative amount of chromium present in the fresh catalysts was investigated by XPS for samples that had been stored under ambient air. Spectra were measured with a Vacuum Generators XPS system, using a CLAM-2 hemispherical analyzer for electron detection. Nonmonochromatic Al $K\alpha$ X-rays, together with an anode current of 20 mA at 10 keV, were used to excite the photoelectron spectra. The pass energy of the analyzer was set at 50 eV and data were collected at intervals of 0.1 eV. Survey spectra were taken with a pass energy of 100 eV at intervals of 0.5 eV. Binding energies are reported with the Al 2p band at 74.7 eV as reference.

The coverage of alumina by chromia was calculated by an XPS analysis program (Debye Institute, Utrecht University, The Netherlands) for the **8-6**, **10-6**, and **12-6** samples. The Cr/Al band intensity ratios, surface areas of the catalysts, and chromium contents were used as input parameters. The calculation assumes that uniform chromia clusters cover the alumina support (31).

Electron Spin Resonance Spectroscopy

The presence of Cr^{3+} and Cr^{5+} in the samples was investigated by ESR. The samples were placed in a quartz cell equipped with a side arm for the ESR measurements. *X*-band spectra were recorded at room temperature and −153°C with Bruker ESP 300 E equipment. A spectrum of the empty cavity was subtracted from the sample spectra. Samples were investigated under dry nitrogen (i) after oxidation overnight at 550°C with O_2 and (ii) after subsequent reduction overnight at 550°C with H_2. For reference, an ESR spectrum was measured for a commercial chromia/alumina catalyst sample (20 wt% Cr) that had been accidentally overheated in excess of 1200°C.

Isoelectric Point Measurements

To assess the acidity of the alumina as a function of the heat treatment, isoelectric point (IEP) was measured for the different alumina supports. Suspensions of 1% alumina support were placed in an ultrasonic bath for 2 h. After, ultrasonication clear solutions were obtained, which were electrophoretically analyzed using a Malvern Instruments Zetamaster S instrument.

RESULTS

Physicochemical Characteristics of the Catalysts

The chromia/alumina samples (4 wt% Cr), whose alumina precalcination temperatures and catalyst calcination temperature were varied, are defined in Table 1. The samples that had been calcined at 600°C were brown, and they turned green and light green when the temperature was increased to 1200°C. Increasing the alumina precalcination temperature caused the color to be more gray; the **12-12** sample was light gray with a shade of ruby red.

The results for the nitrogen physisorption measurements are reported in Table 1. As expected, the surface area of alumina decreased when the precalcination temperature was increased from 800 to 1200°C. During impregnation, the surface area stayed more or less constant. For the **8-*** and **10-*** series, the decrease in surface area during calcination at temperatures 800, 1000, and 1200°C was less than the decrease for alumina. For the **12-*** series, there was a steady decrease in surface area as the calcination temperature was raised, and the lowest surface area of all was for the **12-12** sample. The pore volume of alumina decreased consistently with increasing precalcination temperature. The pore volume of the chromia/alumina samples remained more or less constant up to a calcination temperature of 1000°C, after which it dropped sharply. When the calcination temperature reached 1200°C, the pores of alumina collapsed to a pore volume level below that of chromia/alumina samples prepared on alumina precalcined at 800 and 1000°C.

The X-ray diffractograms measured for the alumina supports are shown in Fig. 2A, and the phases present in the samples are summarized in Table 1. The observed phase change from γ-alumina through θ-alumina to α-alumina is in accord with the literature (32). Note that δ-alumina may have formed from γ-alumina before the detection of θ-alumina, without having been detected; the peaks of γ-alumina and δ-alumina are too close to be separated when the peaks are broadened by the small crystallite size.

The X-ray diffractograms of chromia/alumina samples are shown in Figs. 2B–2D. Alumina phases were identified in all X-ray diffractograms. In the **8-*** series, only γ-alumina was seen after calcination at 600°C. Small amounts of θ-alumina were initially seen at 900°C, and a small amount

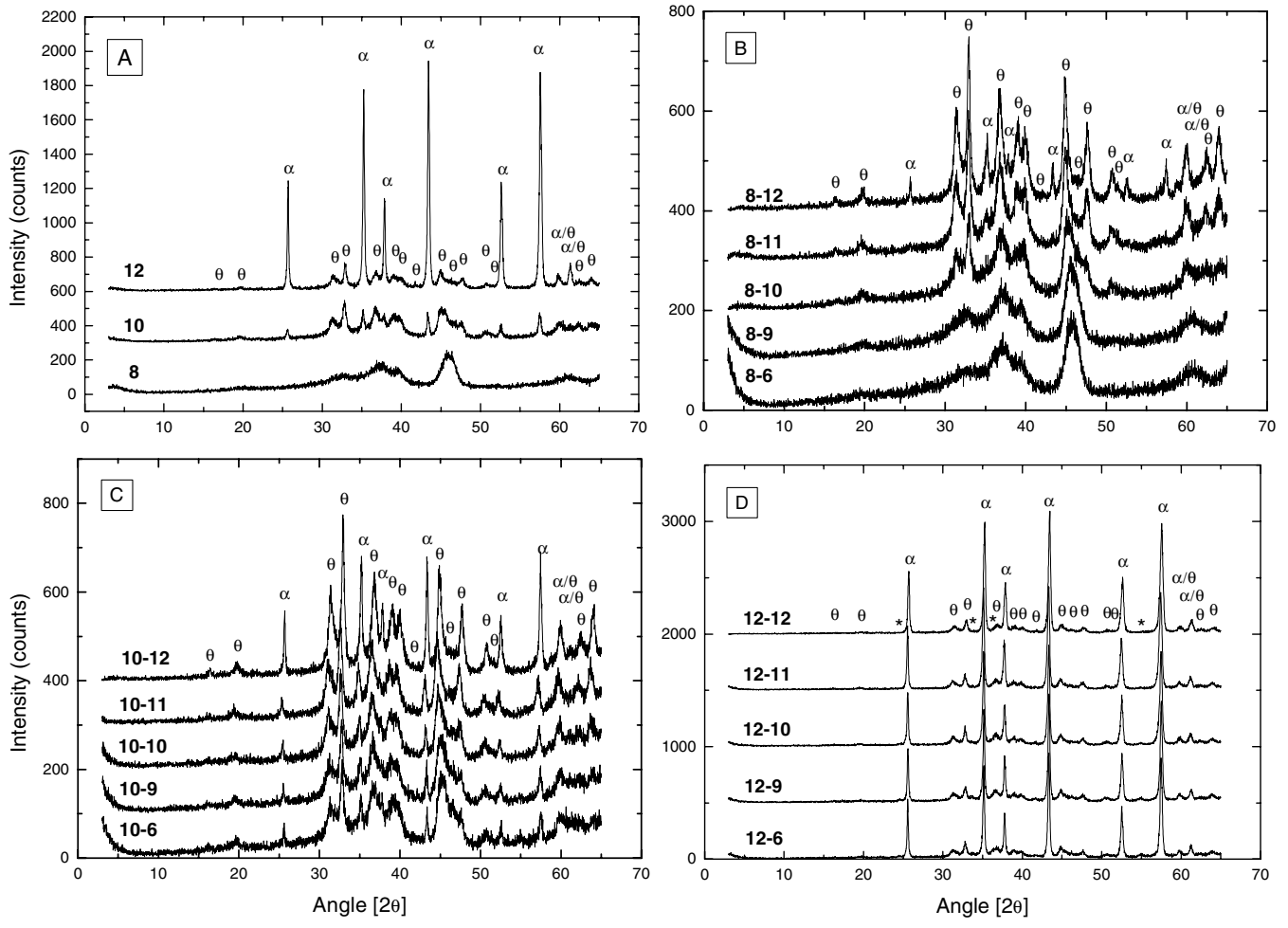

FIG. 2. X-ray diffractograms measured for (A) the alumina samples, (B) the **8-*** series, (C) the **10-*** series, and (D) the **12-*** series of samples. For clarity, curves have been shifted vertically by 300, 100, 100, and 500 counts in A, B, C, and D, respectively. In (D), the four main peaks of α-Cr_2O_3 are marked with symbol *.

of α-alumina was seen at 1200°C. For the **10-*** series, all the X-ray diffractograms were similar, with traces of γ-alumina, much θ-alumina, and some α-alumina. The X-ray diffractograms measured for the **12-*** series likewise were similar to each other and resembled the diffractogram of alumina calcined at 1200°C. For the chromia/alumina samples calcined at 1200°C, the lower the precalcination temperature, the smaller the amount of α-alumina. No peaks of crystalline chromia or of chromia–alumina solid solution were seen in the X-ray diffractograms, except for very weak peaks for samples **12-6**, **12-9**, and **12-10**.

Both the nitrogen physisorption and XRD measurements showed the sintering of alumina to be more pronounced for the alumina support alone than for the chromia/alumina samples. Sintering was seen as a phase transformation from γ-alumina through θ-alumina to α-alumina and as the loss of surface area. In particular, the **8-*** series was resistant to sintering. Our result is in accord with the observations of Simon *et al.* (33), who found that the presence of chromia inhibits the transformation of γ-alumina to α-alumina at temperatures up to 860°C. However, it is contradictory to the conclusion of Vuurman *et al.* (17) and El-Shobaky *et al.* (34) that the presence of chromia on alumina enhances sintering. The reason for the different findings remains unclear.

The chromium contents calculated per unit surface area of the samples, denoted as surface loading, are reported in Table 1. The values lie between 2.5 and 16.0 at_{Cr}/nm^2 (chromium ions per square nanometer of sample). Some are thus below and some above the surface density of chromium on crystalline CrO_3 and on Cr_2O_3, about 4.7 and 10.8 at_{Cr}/nm^2, respectively (24, 35).

Dehydrogenation Activity of Catalysts with 4 wt% Cr

Propene yields obtained with the various 4 wt% catalysts after 4 min on stream are shown in Fig. 3A. Calcination at temperatures up to 1200°C resulted in a loss of activity for

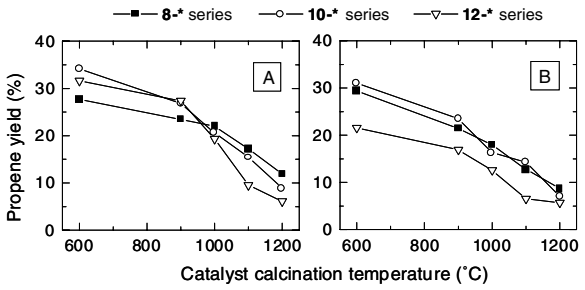

FIG. 3. Propane dehydrogenation activity of the different chromia/alumina catalysts (A) after 4 min and (B) after 17.1 min on stream.

all the catalysts. However, there were differences in the deactivation behavior of the catalysts prepared on different aluminas. After 4 min on stream (Fig. 3A) the activity order was **12-*** ≈ **10-*** > **8-*** for calcination below 900°C and **8-*** > **10-*** > **12-*** for calcination above 900°C. This shows that the **10-*** and **12-*** series were less resistant to deactivation than the **8-*** series upon calcination above 900°C.

The deactivation behavior of the catalyst during time of propane on stream varied with the catalyst. As seen by comparing Figs. 3A and 3B, the **10-*** and **12-*** series deactivated rapidly during time on stream, and after 17 min of propane on stream the activity order was **8-*** ≥ **10-*** > **12-*** for all calcination temperatures. Deactivation during time on stream was least notable for the **8-*** series, but with increasing catalyst calcination temperature even the **8-*** series started deactivating.

We note that the probe of the *in situ* DR spectrometer was present in the reactor during the catalysis runs. The outer surface of the probe is made of stainless steel. To determine whether the high-temperature probe had catalytic activity, the activity of **8** alumina was measured in the presence and absence of the probe. With the probe, propane conversion and propene yield were 8.1 and 0.5%, respectively, whereas without the probe they were 4.5 and 0.6%. Thus, the probe converted propane, but it did not have dehydrogenation activity.

Ex Situ Diffuse Reflectance Spectroscopy

Ex situ DR spectra were measured for the chromia/alumina samples to investigate to what extent incorporation of Cr^{3+} in alumina had taken place during the calcination of the catalysts. Incorporation should be seen as a shift in the positions of the two d–d bands of Cr^{3+} : Cr^{3+} in chromia-type species (not incorporated in alumina), and Cr^{3+} incorporated into alumina absorb at different wavenumbers, as presented in Table 2.

Spectra of sample **8-12** are shown as an example in Fig. 4. The spectra of other samples showed similar bands. The spectra of sample **8-12** in its hydrated and calcined form showed an intense Cr^{6+} charge transition (18, 36) at about 26,000 cm^{-1}. There was also a shoulder caused by the first d–d transition of Cr^{3+} (18; see also 29, p. 111) at about

TABLE 2

Information about Cr^{3+} Species Provided by Different Characterization Methods

Method	Cr^{3+} not incorporated in alumina[a]		Cr^{3+} incorporated in alumina	
	Cr^{3+} exposed on the surface (type 1)	Cr^{3+} inside chromia crystallites (type 2)	Cr^{3+} entrapped in alumina (type 3)	Cr^{3+} migrated into alumina (type 3)
N_2 physisorption	—	—	Large decrease in surface area indicates sintering and formation of these species	—
XRD	Chromia crystallites can be seen		Crystallites of chromia/alumina solid solution can be seen	
Ex situ DRS	Fraction of these species of total Cr^{3+} content can be estimated from d–d bands at 16,600 and 21,700 cm^{-1} (37)		Fraction of these species of total Cr^{3+} content can be estimated from d–d bands at 18,150 and 24,700 cm^{-1} (37)	
In situ DRS	Presence or absence of these species is indicated[b]		Presence or absence of these species is indicated[b]	
XPS	Increase in the amount of species relative to the amount of species in the sample calcined at 600°C is indicated when the Cr/Al band intensity ratio, with increasing catalyst calcination temperature:			
	increases	decreases	stays constant[c]	decreases
ESR	δ-signal indicates presence of type 1′; β-signal may indicate presence of type 1″	β-signal may indicate presence	—[d]	—[d]

[a] Defined as the difference between total Cr^{3+} content and the content of alumina-incorporated Cr^{3+}.
[b] In principle, similar spectral information obtainable as from *ex situ* DRS.
[c] Constant Cr/Al band intensity ratio with decreasing surface area.
[d] No signal could be assigned, but we could not exclude the origin of the κ-signal in type 3 sites.

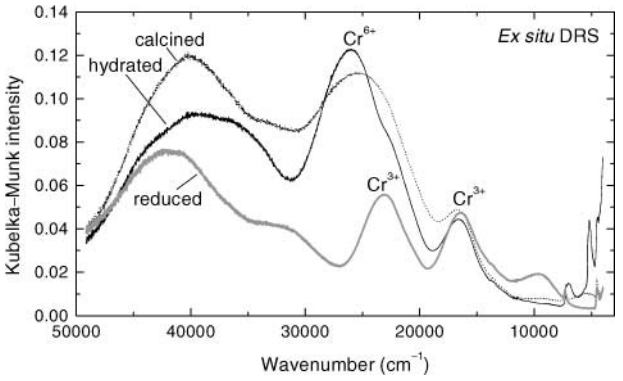

FIG. 4. Examples of *ex situ* DR spectra measured at room temperature under nitrogen for the **8-12** sample in its hydrated, oxidized (O_2 at 550°C), and reduced form (H_2 at 550°C).

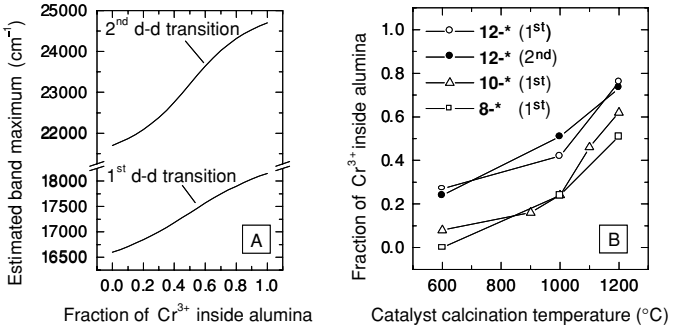

FIG. 5. *Ex situ* DRS investigation of the incorporation of chromium inside alumina. (A) Calculated maxima for the summed d–d bands of Cr^{3+} not incorporated into alumina (16,600 and 21,700 cm^{-1}) and Cr^{3+} incorporated into alumina (18,150 and 24,700 cm^{-1}). (B) Estimated fraction of alumina-incorporated Cr^{3+} of the total Cr^{3+} for the samples.

16,700 cm^{-1}. In the spectrum of the reduced **8-12** sample, the Cr^{6+} band was not present, and the two d–d transitions of Cr^{3+} were well resolved. A third band could be seen in all samples at about 10,000 cm^{-1}. This may indicate the presence of Cr^{3+} in distorted coordination, for example low-coordinated Cr^{3+} species, or the presence of Cr^{2+} (18, 38). The maxima of the three bands in the sample spectra are reported in Table 3. A shift in the Cr^{3+} d–d bands to higher frequencies was observed with increasing catalyst calcination temperature.

We now estimate the fraction of Cr^{3+} incorporated in alumina (type 3 sites) of the total Cr^{3+} content from the positions of the d–d transitions of Cr^{3+} in the *ex situ* DR spectra. For the estimation we assume that (i) the extinction coefficients and the bandwidths are the same for alumina-incorporated Cr^{3+} (type 3) and Cr^{3+} not incorporated into alumina (types 1 and 2 together), and (ii) the d–d transition bands can be approximated by Gaussian functions. Both assumptions should be physically acceptable. From our spectra and from the literature (18) we estimated values for the widths of the first and second d–d transition to be about 4000 and 6000 cm^{-1}, respectively.

The expected maxima of the summed Cr^{3+} d–d bands for a certain fraction of alumina-incorporated Cr^{3+} are displayed in Fig. 5A. By comparing the observed maxima against the expected positions, we can estimate the fraction of alumina-incorporated Cr^{3+}. The results are shown in Fig. 5B. The extent of incorporation of Cr^{3+} in alumina

TABLE 3

Summary of the *Ex Situ* DRS, XPS, ESR, and Activity Results for the Chromia/Alumina Catalysts

Sample code	Bands detected in *ex situ* DRS[a] (cm^{-1})	XPS Cr 2p/Al 2p band intensity ratio	Signals detected in ESR		Turnover frequency[b] ($molecule_{propene}/(at_{Cr}s)$)
			Oxidized sample	Reduced sample	
8-6	10,400 (sh), 16,400, 23,500	1.27	γ, δ, (β)	γ, δ, (β)	0.0031
8-9	—[c]	1.09	—	—	—
8-10	10,000, 16,900, 23,800	—	—	—	0.0032
8-11	—	—	—	—	—
8-12	9,700, 17,400, 24,000	1.00	γ, δ, (κ)	δ, κ	0.0027
10-6	10,400, 16,700, 22,500	1.81	γ, δ, (β)	(γ), δ, (β)	0.0042
10-9	9,900, 16,800, 22,800	1.43	γ, δ	δ, β, (κ)	0.0036
10-10	9,800, 16,900, 23,400	1.38	γ, δ, (κ)	δ, κ	0.0030
10-11	9,800, 17,300, 23,800	1.25	γ, δ, (κ)	δ, κ	0.0032
10-12	9,800, 17,600, 24,200	1.18	γ, δ, κ	δ, κ	0.0026
12-6	9,800, 16,900, 22,300	3.84	γ, (δ), β	(δ), β	0.0047
12-9	—	2.45	—	—	—
12-10	9,800, 17,400, 23,000	—	—	—	0.0040
12-11	—	—	—	—	—
12-12	10,000, 17,800, 24,200	1.38	κ	κ	0.0027

[a] Apparent maxima in spectra measured for reduced samples.
[b] Turnover frequencies were calculated for 4 min of propane on stream per Cr not incorporated in alumina.
[c] Not applicable or not determined.

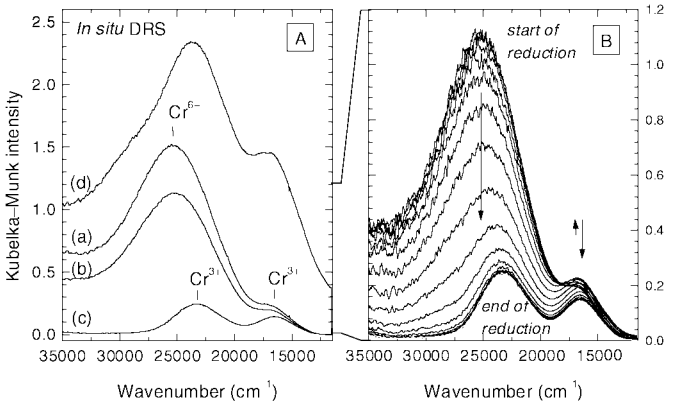

FIG. 6. Examples of *in situ* UV–vis DR spectra measured during the first dehydrogenation cycle for the **8-11** sample. (A) Spectra collected in 50 s (1000 scans of 50 ms): (a) after heating to 580°C in oxygen, (b) after subsequent helium flush, (c) during the propane feed (21 s from the start of the reaction), and (d) during the propane feed (6 min from the start of the reaction). (B) Spectra collected in 1 s (20 scans of 50 ms) during the propane feed (up to 21 s of the reaction). (Spectra have not been smoothed.)

increased with the catalyst calcination temperature and alumina precalcination temperature. For the **8-*** and **10-*** series, strong background absorption shifted the positions of the second d–d transitions to higher energy, so that they could not be used for the estimation. For the **12-*** series, background absorption was low, and the second d–d transitions could be used for the estimation. As can be seen in Fig. 6B, the fractions of alumina-incorporated Cr^{3+} estimated for the **12-*** series from the first and second d–d transitions agreed within ±0.05, indicating the reliability of the estimation procedure.

From the total chromium loading (4 wt% Cr), the estimated fraction of alumina-incorporated Cr^{3+} (Fig. 5B), and the surface area of the samples, we could calculate the surface loading of chromium that was not incorporated into alumina and was available for catalysis. These values are reported in Table 1. The surface loading of nonincorporated Cr^{3+} stayed more or less constant for the **8-*** series, decreased slightly after calcination above 1000°C for the **10-*** series, and decreased steadily with increasing calcination temperature for the **12-*** series.

In Situ Diffuse Reflectance Spectroscopy

The catalysts of the **8-*** and **12-*** series were monitored *in situ* by DRS during the dehydrogenation runs to see which oxidation states of chromium were present during catalysis. The behavior of the **8-6**, **8-9**, **8-10**, and **8-11** samples was similar. Figure 6A shows spectra measured for the **8-11** sample as an example. Cr^{6+} was present after the heating of the sample to the reaction temperature (580°C), as shown by the Cr^{6+} charge transfer band centered at about 25,600 cm^{-1} (see curve a). Cr^{3+} was also present, seen as a shoulder around 17,000 cm^{-1}. (Note that increased measurement temperature shifts the band maxima to a lower wavenumber.) During the following helium flush, the intensity of the Cr^{6+} band decreased slightly, indicating that not all the Cr^{6+} was stable (curve b).

When propane was introduced, Cr^{6+} was reduced and the Cr^{6+} band disappeared (Fig. 6A, curve c). Spectra measured during reduction are shown in Fig. 6B, and the intensity at 26,000 cm^{-1} as a function of time is reported in Fig. 7A. The Cr^{6+} was reduced in about 10 s and the two d–d transitions of Cr^{3+} became resolved at 16,500 and 23,500 cm^{-1}, as shown in curve c of Fig. 6A. The d–d band maxima of Cr^{3+} shifted to higher energy with increasing catalyst calcination temperature and alumina precalcination temperature, in accord with the results of *ex situ* DRS. After reduction, coke formation began, as seen in the increased background absorption (see Fig. 7B and curve d in Fig. 6A). No indication of Cr^{2+} around 10,000 cm^{-1} was seen in the spectra, but the spectrum did not extend to sufficiently low wavenumbers to allow us to exclude its presence.

Coke was removed during the oxidative regeneration in about 3 min (see Fig. 7C), as seen from a decrease in the background absorption. A spectrum typical of Cr^{6+} with a band at 25,700 cm^{-1} was formed, with a shoulder due to Cr^{3+}. The Cr^{6+} band continued to intensify during the whole oxidative regeneration (see Fig. 7D) without obtaining the original intensity. The spectroscopic features of the second and third dehydrogenation cycles resembled those of the first cycle, with the exception that the Cr^{6+} was reduced to Cr^{3+} during the helium flush preceding dehydrogenation.

The spectra of the **8-12** sample differed from those of other samples of the 8–∗ series but they resembled the

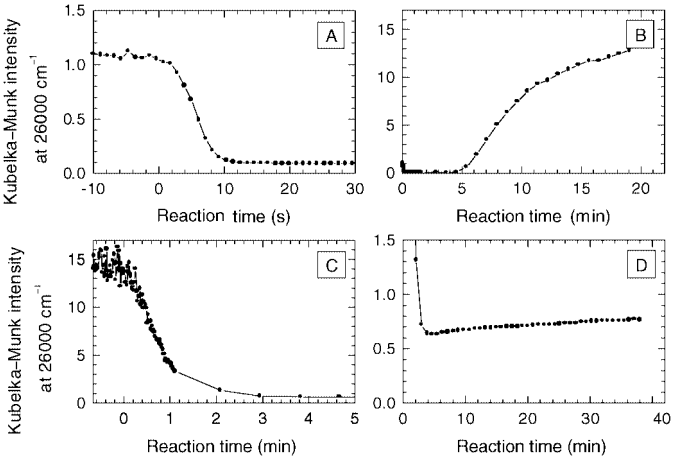

FIG. 7. Intensity at 26,000 cm^{-1} of the *in situ* UV–vis DR spectra measured for the **8-11** catalyst during the first cycle for (A) the start of the propane feed (spectra shown in Fig. 6B), (B) during the 20 min of propane feed, (C) at the start of oxidative regeneration, and (D) during the 40 min of oxidative regeneration. Zero time marks the start.

spectra measured for the **12-*** series. The band of Cr^{6+} was not present in any of these spectra. Well-resolved d–d transitions of Cr^{3+} were present, and coke formation appeared as increased background intensity during dehydrogenation.

X-Ray Photoelectron Spectroscopy

XPS measurements were carried out to investigate the surface concentration of chromium in the fresh catalysts. The Cr/Al band intensity ratios are given in Table 3. For samples calcined at 600°C, the ratio increased with the alumina precalcination temperature, as expected for increasing surface loading of chromium (see Table 1). The coverage of alumina by chromia was calculated as 70, 77, and 97% for the **8-6**, **10-6**, and **12-6** samples, respectively, and the corresponding thickness of the chromia layer was calculated as 1.2, 2.8, and 5.1 Å. The chromia layer was thus well dispersed over alumina.

The Cr/Al band intensity ratio decreased with increasing calcination temperature, indicating that chromium was lost from the surface. This was minor for the **8-*** series (decrease by 21% during calcination to 1200°C), more notable for the **10-*** series (45%), and most pronounced for the **12-*** series (64%). Two processes (or their combined effect) could account for the decrease in the Cr/Al band intensity ratio: (i) an increase in the size of chromia crystallites (sintering of chromia) or (ii) incorporation of Cr^{3+} into the alumina support through migration, that is, mixing of phases. Incorporation through entrapment during sintering of the alumina support should not decrease the Cr/Al band intensity ratio.

Electron Spin Resonance Spectroscopy

ESR measurements were carried out to investigate the effect of calcination treatments on the chromium species. Typically, three ESR resonances are reported for chromia/alumina: the γ-, β-, and δ-signal (5, 6, 22, 39). The γ-signal is centered at about $g = 1.97$, has a width of about 50–60 G, and originates from isolated Cr^{5+} species that are stabilized on the surface of alumina in square–pyramidal symmetry (5, 6, 22). The β-signal originates from Cr_2O_3 clusters of small dimensions; widths between 800 and 1800 G and $g = 1.95$–1.98 have been reported (5, 6, 22). The β-signal becomes narrower and shifts to a lower g factor with increasing cluster size (40), with the values finally approaching those of α-chromia ($g = 1.98$, width about 500 G (5)). α-Chromia, however, has a Néel temperature of 34°C and cannot be seen in spectra measured at or below room temperature (6). The δ-signal originates from isolated Cr^{3+} in distorted octahedral coordination. It is a broad signal, with contributions at about $g = 2.2$ (5) and 2.5–4.3 (22). There is no general agreement in the literature on the exact origin of the δ-signal: catalytically active surface Cr^{3+} species (25) and catalytically inactive alumina-incorporated Cr^{3+} species (6) have both been concluded. We will attempt to clarify this inconsistency.

ESR spectra were measured for samples in their oxidized and reduced forms at room temperature and at −153°C. Spectra for the samples calcined at 1200°C are shown in Fig. 8. The presence or absence of the γ-, β-, and δ-signals in the sample spectra is summarized in Table 3. The γ-signal, which originates from Cr^{5+}, was observed in almost all the spectra of oxidized samples, with a position of typically $g = 1.97$ and a width of 70–90 G. The signal seemed to be less intense the higher the alumina precalcination temperature, and in the extreme case of the **12-12** sample, no γ-signal could be seen. Thus, the amount of Cr^{5+} seemed to decrease with increasing precalcination temperature. In the spectra of reduced samples, the γ-signal signal was typically either absent or considerably decreased in intensity. Hydrogen treatment at 550°C thus reduced Cr^{5+} to lower oxidation states, as indicated also by the *ex situ* DRS measurements. However, for some samples, especially **8-6**, the signal increased during the reduction step, indicating stabilization

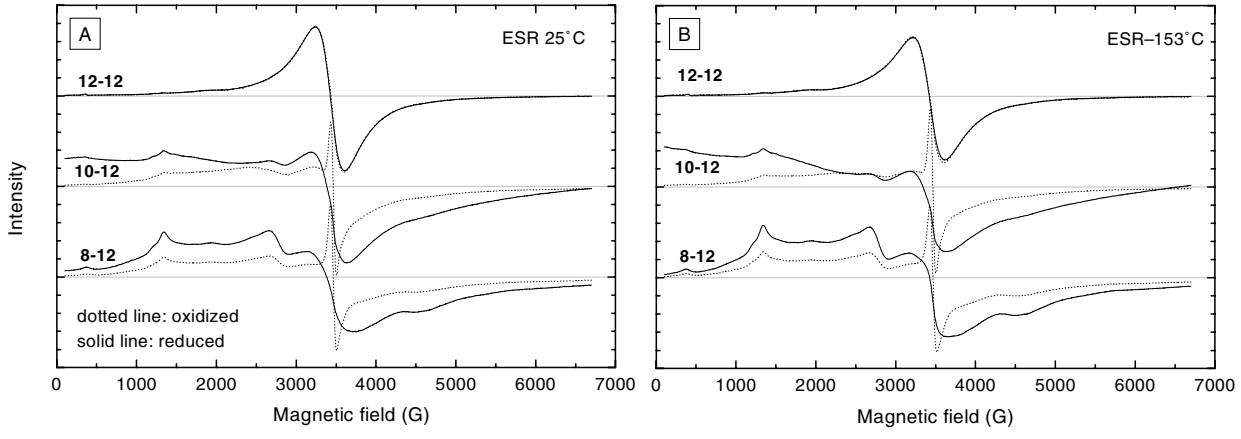

FIG. 8. ESR spectra measured for the **8-12**, **10-12**, and **12-12** samples in oxidized and reduced form (A) at room temperature and (B) at −153°C.

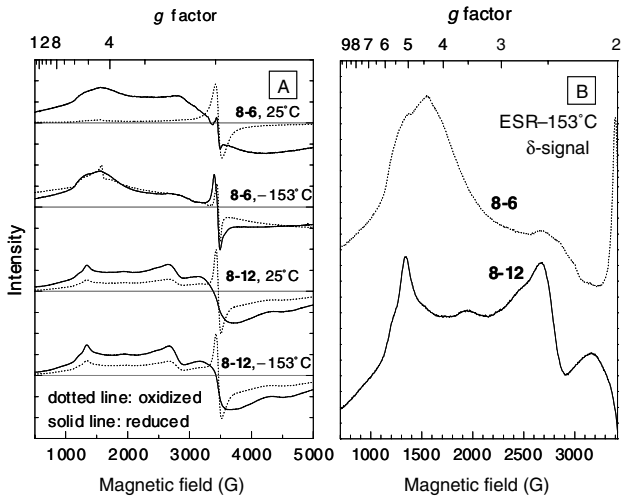

FIG. 9. ESR spectra for the **8-6** and **8-12** samples (A) measured at room temperature and at −153°C in oxidized and reduced form, and (B) measured at −153°C in reduced form, shown with the region of the δ-signal magnified.

of Cr^{5+} species. Our results are in accord with literature reports that some Cr^{5+} ions are stable in hydrogen but are reduced by alkanes (25, 41).

In the spectra of the **8-6**, **10-6**, and **12-6** samples, the β-signal became narrower with increasing alumina precalcination temperature. This is in line with the increase in the surface loading of chromium with increasing alumina precalcination temperature (see Table 1); higher surface loading should result in larger size of the chromia clusters and thus a narrower β-signal. In the other sample spectra, the β-signal was generally very wide or absent (see Table 2). There was no indication that the β-signal became narrower with increasing catalyst calcination temperature. Thus, the decrease in dispersion with increasing calcination temperature suggested by XPS was not confirmed by ESR.

The δ-signal was observed for all samples except **12-12** (see Table 3). Comparison of the different ESR spectra (examples are shown in Fig. 9A) showed that the δ-signal is highly complex. It consisted of two main maxima: one located at $g \approx 4.0$–5.5 and the other at $g \approx 2.6$. In addition, there may have been a small hump at $g \approx 3.5$. The observed signal position is generally in accord with the literature values (5, 22, 33). Moreover, simulations of the δ-signal have suggested that a maximum should appear at $g \approx 2$ (40). Even though the position of the δ-signal was constant in the sample spectra, its appearance was not. For samples calcined at low temperature, the signal was wide and the contribution at $g \approx 2.6$ was indistinct, whereas for samples calcined at high temperatures, the maxima were sharp and the contribution at $g \approx 2.6$ was clearly seen.

There is disagreement in the literature on the origin of the δ-signal: it originates either (i) from alumina-incorporated Cr^{3+} or (ii) from isolated, catalytically active Cr^{3+} surface species. Our current and earlier (18) *in situ* and *ex situ* DRS measurements have confirmed that the extent of incorporation of Cr^{3+} into alumina increases with catalyst calcination temperature and alumina precalcination temperature. Thus, if the δ-signal originated from alumina-incorporated Cr^{3+}, we would expect its intensity to have increased with the catalyst calcination temperature. The intensity was analyzed for the **10-*** series, but no trend was observed. Furthermore, the intensity decreased with increasing alumina precalcination temperature. We found no evidence, therefore, that the δ-signal originated from alumina-incorporated Cr^{3+}.

Several pieces of evidence suggest that the δ-signal originates from surface Cr^{3+} species. (i) In accordance with earlier observations (5, 25, 42), the intensity of the signal increased during reduction of the samples (see Figs. 8 and 10A). This suggests that part of the Cr^{3+} responsible for the δ-signal formed through the reduction of chromium in higher oxidation states (Cr^{6+} and Cr^{5+}). Relevant to this, Simon *et al.* (33) observed the reverse process: during oxidation, Cr^{5+} (γ-signal) was formed from the Cr^{3+} responsible for the δ-signal. Reduction–oxidation treatments are expected predominantly to affect surface species. (ii) Further evidence for the surface Cr^{3+} species is that the appearance of the signal varied with the sample type (see the comparison in Fig. 9B). The coordination environment of surface Cr^{3+} species may change when the sample type changes, and this could affect δ-signal. (iii) The intensity of the δ-signal also decreased with increasing precalcination temperature of alumina. The number of sites where Cr^{3+} can be stabilized in isolated positions presumably is more or less constant per unit surface area, so that in the **8-12**, **10-12**, and **12-12** samples the ratio of sites for isolated Cr^{3+} is about 2.5 : 2.0 : 1.0. The marked increase in chromium loading per square nanometer with the alumina precalcination temperature (see Table 1) could be expected to further decrease the amount of isolated Cr^{3+} sites. We would thus expect considerably higher concentrations of isolated Cr^{3+} species on aluminas precalcined at lower temperatures. This type of behavior was seen for the δ-signal. We conclude, in accord with Brückner *et al.* (25), that the δ-signal originates from isolated Cr^{3+} surface sites. The δ-signal intensities indicate that the order of abundance of isolated Cr^{3+} sites in the samples calcined at 600°C was **8-6** ≫ **10-6** > **12-6**.

In addition to the γ-, β-, and δ-signals, our spectra presented a fourth signal, which, to our knowledge, has not been reported before. This signal had a symmetric lineshape with a center at $g = 2.00$–2.01 and a width of ∼350–500 G. It is denoted "κ" in Table 3. The κ-signal was most intense and most clearly resolved—because of the absence of other signals—in the spectra measured for the **12-12** sample, shown in Fig. 8. The signal intensity appeared to decrease slightly with a decrease in the measurement

temperature, but the linewidth remained constant. The unchanging linewidth distinguishes the κ-signal from the β-signal. Reduction with hydrogen did not affect the intensity of the signal. Since this signal was observed in the reduced samples, we conclude that it probably originated from some Cr^{3+} species. The symmetric lineshape indicates well-defined octahedral environment and the position and linewidth resemble those reported for α-Cr_2O_3. However, since α-Cr_2O_3 should not be seen at temperatures below room temperature (5), the signal cannot originate from α-Cr_2O_3. A reference ruby-type chromia/alumina sample had a similar ESR spectrum, suggesting that a mixed chromia–alumina phase or isolated Cr^{3+} located inside alumina could be responsible for the κ-signal. In future, simulations and multifrequency ESR measurements would help to clarify the origin of the κ-signal.

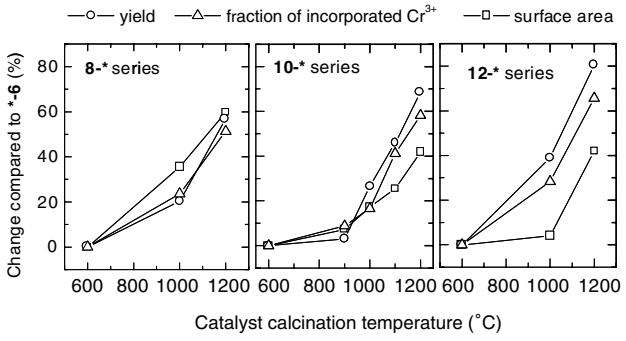

FIG. 10. Changes with increasing catalyst calcination temperature compared with the results for catalyst calcined at 600°C: (A) decrease in yield, (B) increase in the fraction of alumina-incorporated Cr^{3+} (as estimated from the *ex situ* DRS results), and (C) decrease in surface area.

DISCUSSION

Deactivation during Calcination at High Temperatures

Calcination of the chromia/alumina catalysts at high temperatures (up to 1200°C) led to their deactivation (see Fig. 3). The catalysts prepared on alumina precalcined at 800°C deactivated the least. Three factors could have caused the deactivation with increasing calcination temperature: (i) the turnover frequency per exposed chromium ion could have decreased, (ii) the chromia crystallites could have sintered, generating inactive Cr^{3+} sites of type 2, or (iii) chromium could have incorporated inside alumina, generating inactive Cr^{3+} sites of type 3 (see Fig. 1a, for types of Cr^{3+} sites).

We do not consider it likely that the turnover frequency of the chromium sites decreased drastically enough to explain the drop in activity with increasing catalyst calcination temperature. It has been found that the dehydrogenation activity of chromia/alumina catalysts increases more or less linearly with chromium loading up to a surface loading of 10–12 at_{Cr}/nm^2; beyond this it decreases (7, 10). The finding indicates that the catalytic activity of the different sites (types 1′ and 1″ or redox Cr^{3+} and nonredox Cr^{3+}) should be of the same order of magnitude. It also seems improbable that sintering of chromia with increasing catalyst calcination temperature could explain the drastic decrease in activity, since the spectroscopic characterization by ESR and XRD did not reveal much increase in the cluster size of chromia. (XPS indicated that surface chromium species were lost during calcination of the catalysts, but it could not differentiate between the two processes of sintering of chromia and incorporation of chromium into alumina.)

To investigate whether incorporation of Cr^{3+} inside the alumina support could explain the observed deactivation with increasing catalyst calcination temperature, the percentage decrease in propene yield and percentage increase in the fraction of alumina-incorporated Cr^{3+} (estimated from *ex situ* DRS) as a function of the catalyst calcination temperature are plotted in Fig. 10. The decrease in yield and the increase in the fraction of incorporated Cr^{3+} roughly coincide for all series (**8-***, **10-***, and **12-***). The agreement suggests that incorporation of Cr^{3+} inside the alumina support was the main reason for the deactivation with increasing catalyst calcination temperature.

The incorporation of Cr^{3+} inside alumina could have occurred through two processes. (i) Chromium could have been entrapped inside alumina when the structure of alumina sintered during calcination at high temperatures. (ii) Chromium could have migrated into the alumina during calcination. These processes are schematically illustrated in Fig. 11. The percentage decrease in surface area is plotted as a function of the catalyst calcination temperature in Fig. 10 for the three series. From Fig. 10A we see that, for the **8-*** series, the extent of sintering of the sample (that is, loss of surface area) and the amount of alumina-incorporated Cr^{3+} roughly agree. This indicates that Cr^{3+} was incorporated into alumina mostly through the entrapment process. The XPS results are in line with this conclusion: a minor decrease was observed for the Cr/Al band intensity ratio with increasing catalyst calcination temperature. For the **10-*** series, the extent of sintering and the

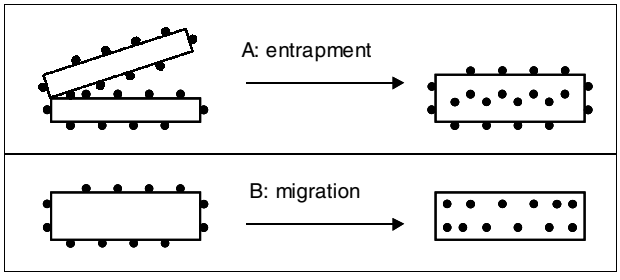

FIG. 11. Schematic representation of the processes leading to the incorporation of Cr^{3+} inside the alumina support: (A) entrapment and (B) migration. (Black dots) Cr^{3+}; (white box) alumina.

amount of alumina-incorporated Cr^{3+} agreed up to a calcination temperature of 1000°C. Beyond 1000°C, the amount of incorporated Cr^{3+} was greater than the extent of sintering. Thus, up to about 1000°C, catalytically active Cr^{3+} was lost mostly through entrapment, and at higher temperatures also through migration. For the **12-*** series, the amount of alumina-incorporated Cr^{3+} seems greater than the extent of sintering, and migration seems to account for the loss of active Cr^{3+}.

We conclude that incorporation of Cr^{3+} into the alumina support took place through two processes: entrapment caused by sintering of the support, and migration of Cr^{3+} into the support. Which of these processes occurred depended on the structure of the alumina support: on samples rich in γ-alumina only entrapment occurred, whereas on samples with practically no γ-alumina migration dominated.

Effect of Support on Dehydrogenation Activity

The type of support affected the activity of the chromia/alumina catalysts: for catalyst calcination at 600°C, samples prepared on **10** and **12** alumina were initially (4 min of propane on stream) significantly more active than the sample prepared on **8** alumina. For a meaningful comparison of these results, with each other and with literature data, we calculated turnover frequencies (TOF). The estimated surface loading of the samples remained below 10.84 at_{Cr}/nm^2 (see Table 1), which is the density of chromium on the surface of α-Cr_2O_3 (35), indicating that all the chromium not incorporated in alumina should have been available for catalysis. The TOFs were calculated per chromium ion type not incorporated in alumina. Thus, the TOFs represent the average values for the different species present on the surface (type 1′, type 1″, and maybe even some type 2 sites).

The TOF values, reported in Table 3, are of the same order of magnitude as those reported by De Rossi *et al.* (5, 6) for chromia/alumina catalysts. For the catalysts calcined at 600°C, the order of the TOFs was **12-6** > **10-6** > **8-6**. With increasing catalyst calcination temperature, TOFs remained approximately constant for the **8-*** series and decreased for the **10-*** and **12-*** series. Furthermore, for catalyst calcination at 1200°C, the TOFs were identical for the **8-***, **10-***, and **12-*** series. The trend in TOF with increasing catalyst calcination temperature would seem to exclude a relationship between the presence of θ-alumina and α-alumina and the activity of the Cr^{3+} sites (which we proposed earlier (21)): had there been a relationship, the TOF values should have increased with the catalyst calcination temperature, but the opposite was observed. The differences in the TOF values seem instead to be due to the different activities of the surface Cr^{3+} species. ESR investigation showed that the **8-6** catalyst sample (alumina-supported chromium, 2.5 at_{Cr}/nm^2) contained the greatest number of isolated Cr^{3+} sites, the **10-6** sample (3.9 at_{Cr}/nm^2) considerably fewer, and the **12-6** sample (6.9 at_{Cr}/nm^2) almost none. Thus, the TOF values increased with a decreasing number of isolated Cr^{3+} (type 1′) sites, that is, with an increasing number of multinuclear (type 1″) Cr^{3+} sites.

Our finding that type 1″ sites are more active in dehydrogenation than type 1′ sites is in full agreement with the results of Brückner *et al.* (25), according to whom multinuclear Cr^{3+} sites (type 1″ sites) are catalytically more active than isolated Cr^{3+} sites (type 1′). It is also in accord with the proposal of Cavani *et al.* (7) and Airaksinen *et al.* (12) that nonredox Cr^{3+} is more active than redox Cr^{3+} in dehydrogenation. Our finding differs from the conclusion of De Rossi *et al.* (5, 6) that mononuclear redox Cr^{3+} is the active dehydrogenation site, and from the conclusion of Hakuli *et al.* (10) that the size of chromia ensembles has no effect. De Rossi *et al.* (6) noted, however, that for higher chromium loadings, clustered (that is, nonredox or type 1″) chromia could have some catalytic activity. Hakuli *et al.* (8, 10) suggested that redox Cr^{3+} could fully account for the dehydrogenation activity up to a surface loading of about 5 $at_{Cr}\ nm^{-2}$, and beyond that nonredox Cr^{3+} must also have dehydrogenation activity. At low chromium loadings (<5 $at_{Cr}\ nm^{-2}$) nonredox Cr^{3+} would not be catalytically active because it is incorporated inside alumina (10). On the basis of our present results, incorporation of Cr^{3+} into γ-alumina during calcination (at ~600°C) seems unlikely, however.

The chromia/alumina catalysts deactivated reversibly during time of propane on stream (compare Figs. 3A and 3B). For catalyst calcination at 600°C, deactivation was most severe in the order **12-6** > **10-6** > **8-6**. Likely reasons for the reversible deactivation could be that (i) active chromia sintered under the presence of propane, resulting in a decreased amount of catalytically active surface chromium, (ii) highly active sites were rapidly blocked by coke formation (43), or (iii) coke formation was dependent on the type of alumina support. According to XPS C/Al band intensity ratios measured for the catalysts, coke formation was strongest for the catalysts in the order **12-6** > **10-6** ≈ **8-6** (C/Al band intensity ratios were 3.1, 1.6, and 1.2, respectively). The acidities of the supports were assessed by measuring their IEPs. The IEPs of the **8**, **10**, and **12** alumina samples were 9.0, 9.0, and 7.8, indicating that the **12** support was more acidic than the other supports. Thus, the reversible deactivation could be explained by coke formation enhanced by the acidity of the alumina support. We cannot exclude, however, the possibility that sintering of chromia or selective coking of active Cr^{3+} species may have occurred.

CONCLUSIONS

Catalytically inactive, alumina-incorporated Cr^{3+} species (type 3) were formed in chromia/alumina catalysts through two processes: (i) entrapment of Cr^{3+} ions inside the

alumina support through sintering of the alumina support, and (ii) migration of Cr^{3+} ions into the alumina support. The amount of alumina-incorporated Cr^{3+} was estimated by DRS measurements. The presence of impregnated chromia inhibited the phase transformation from γ- to α-alumina. The presence of γ-alumina, in turn, hindered the migration of Cr^{3+} ions into the alumina. Our results indicate that the δ-signal in ESR spectra originates from isolated surface Cr^{3+} species that are catalytically active (type 1′ species). The dehydrogenation activity was higher for multinuclear Cr^{3+} sites (type 1″) than for isolated Cr^{3+} (type 1′). No substantial effect of the phase of the alumina support on the dehydrogenation activity could be detected.

Presumably there are differences between the deactivation of chromia/alumina catalysts in this work and use of chromia/alumina catalysts in industry. In this work, inactive species were generated through an oxidative treatment of the catalysts lasting a few days. In industrial use, catalysts are expected to deactivate under both oxidizing and reducing atmospheres at high temperatures during operation of more than a year. The next step would be to investigate the irreversible deactivation of chromia/alumina catalysts with industriallike chromium loadings under reducing conditions.

ACKNOWLEDGMENTS

Kathleen Vanrusselt is thanked for the activity and XRD measurements, Hugo Leeman for the *ex situ* DRS measurements, Bjorn Dieu for the ESR measurements, Ad Mens for the XPS measurements, and André Maes and Kathleen Geraedts for the IEP measurements. Valuable discussions with Outi Krause, Onno Gijzeman, Robert Schoonheydt, and Sanna Airaksinen are gratefully acknowledged. This work was supported by the Academy of Finland through the Graduate School in Chemical Engineering (GSCE) and by Fonds voor Wetenschappelijk Onderzoek—Vlaanderen (FWO).

REFERENCES

1. Buonomo, F., Sanfilippo, D., and Trifirò, F., *in* "Handbook of Heterogeneous Catalysis" (G. Ertl, H. Knözinger, and J. Weitkamp, Eds.), Vol. 5, p. 2140. VCH, Weinheim, 1997.
2. Weckhuysen, B. M., and Schoonheydt, R. A., *Catal. Today* **51**, 223 (1999).
3. Sanfilippo, D., *Cattech* **4**, 56 (2000).
4. Bhasin, M. M., McCain, J. H., Vora, B. V., Imai, T., and Pujadó, P. R., *Appl. Catal. A* **221**, 397 (2001).
5. De Rossi, S., Ferraris, G., Fremiotti, S., Garrone, E., Ghiotti, G., Campa, M. C., and Indovina, V., *J. Catal.* **148**, 36 (1994).
6. De Rossi, S., Pia Casaletto, M., Ferraris, G., Cimino, A., and Minelli, G., *Appl. Catal. A* **167**, 257 (1998).
7. Cavani, F., Koutyrev, M., Trifirò, F., Bartolini, A., Ghisletti, D., Iezzi, R., Santucci, A., and Del Piero, G., *J. Catal.* **158**, 236 (1996).
8. Hakuli, A., Kytökivi, A., Krause, A. O. I., and Suntola, T., *J. Catal.* **161**, 393 (1996).
9. Kytökivi, A., Jacobs, J.-P., Hakuli, A., Meriläinen, J., and Brongersma, H. H., *J. Catal.* **162**, 190 (1996).
10. Hakuli, A., Kytökivi, A., and Krause, A. O. I., *Appl. Catal. A* **190**, 219 (2000).
11. Hakuli, A., Ph.D. thesis. Helsinki University of Technology, 1999.
12. Airaksinen, S. M. K., Kanervo, J. M., and Krause, A. O. I., *Stud. Surf. Sci. Catal.* **136**, 153 (2001).
13. Kanervo, J. M., and Krause, A. O. I., *J. Catal.* **207**, 57 (2002).
14. Gorriz, O. F., and Cadús, L. E., *Appl. Catal. A* 180, 247 (1999).
15. Mentasty, L. R., Gorriz, O. F., and Cadús, L. E., *Ind. Eng. Chem. Res.* **38**, 396 (1999).
16. Mentasty, L. R., Gorriz, O. F., and Cadús, L. E., *Ind. Eng. Chem. Res.* **40**, 136 (2001).
17. Vuurman, M. A., Hardcastle, F. D., and Wachs, I. E., *J. Mol. Catal.* **84**, 193 (1992).
18. Weckhuysen, B. M., Wachs, I. E., and Schoonheydt, R. A., *Chem. Rev.* **96**, 3327 (1996).
19. Weckhuysen, B. M., Bensalem, A., and Schoonheydt, R. A., *J. Chem. Soc. Faraday Trans.* **94**, 2011 (1998).
20. Weckhuysen, B. M., Verberckmoes, A. A., Debaere, J., Ooms, K., Langhans, I., and Schoonheydt, R. A., *J. Mol. Catal. A* **151**, 115 (2000).
21. Puurunen, R. L., Beheydt, B. G., and Weckhuysen, B. M., *J. Catal.* **204**, 253 (2001).
22. Khaddar-Zine, S., Ghorbel, A., and Naccache, C., *J. Mol. Catal. A* **150**, 223 (1999).
23. Brückner, A., *Chem. Commun.* 2122 (2001).
24. Grzybowska, B., Słoczyński, J., Grabowski, R., Wcisło, K., Kozłowska, A., Stoch, J., and Zieliński, J., *J. Catal.* **178**, 687 (1998).
25. Brückner, A., Radnik, J., Hoang, D.-L., and Lieske, H., *Catal. Lett.* **60**, 183 (1999).
26. Cimino, A., Cordischi, D., De Rossi, S., Ferraris, G., Gazzoli, D., Indovina, V., Occhiuzzi, M., and Valigi, M., *J. Catal.* **127**, 761 (1991).
27. Weckhuysen, B. M., Schoonheydt, R. A., Jehna, J.-M., Wachs, I. E., Cho, S. J., Ryoo, R., Kijlstra, S., and Poels, E., *J. Chem. Soc. Faraday Trans.* **91**, 3245 (1995).
28. Dietz, W. A., *J. Gas Chromatogr.* **5**, 68 (1967).
29. Burns, R. G., "Minerological Applications of Crystal Field Theory," 2nd ed. Cambridge Univ. Press, Cambridge, UK, 1993.
30. Weckhuysen, B. M., *Chem. Commun.* 97 (2002).
31. Kuipers, H. P. C. E., *Solid State Ionics* **16**, 15 (1985).
32. Morterra, C., and Magnacca, G., *Catal. Today* **27**, 497 (1996).
33. Simon, S., van der Pol, A., Reijerse, E. J., Kentgens, A. P. M., van Moorsel, G.-J. M. P., and de Boer, E., *J. Chem. Soc. Faraday Trans.* **91**, 1519 (1995).
34. El-Shobaky, H. G., Ghozza, A. M., El-Shobaky, G. A., and Mohamed, G. M., *Colloids Surf. A* **152**, 315 (1999).
35. Lugo, H. J., and Lunsford, J. H., *J. Catal.* **91**, 155 (1985).
36. Lever, A. B. P., "Inorganic Electronic Spectroscopy," 2nd ed. Elsevier, Amsterdam, 1984.
37. Deleted in proof.
38. Scarano, D., Spoto, G., Bordiga, S., Carnelli, L., Ricchiardi, G., and Zecchina, A., *Langmuir* **10**, 3094 (1994).
39. Poole, C. P., and MacIver, D. S., *Adv. Catal.* **17**, 262 (1967).
40. Weckhuysen, B. M., Ph.D. thesis. Katholieke Universiteit Leuven, 1995.
41. Selwood, P. W., *J. Am. Chem. Soc.* **92**, 39 (1970).
42. Weckhuysen, B. M., De Ridder, L. M., Grobet, P. J., and Schoonheydt, R. A., *J. Phys. Chem.* **99**, 320 (1995).
43. Masson, J., and Delmon, B., *in* "Proceedings, 5th International Congress on Catalysis, Palm Beach, 1972" (J. W. Hightower, Ed.), p. 183. North Holland, Amsterdam, 1973.